OPTICAL SENSOR CALIBRATION USING SIMULATED RADIANCES OVER DESERT SITES

*Y. Govaerts**

Consultant for VITO,
ygovaerts@gmail.com
Brussels, Belgium

S. Sterckx, S. Adriaensen

Centre for Remote Sensing and Earth Observation
VITO
Boeretang 200, 2400 Mol, Belgium

ABSTRACT

This paper presents the improvements of an absolute calibration reference system based on simulated TOA BRF time series over bright desert targets. The current work highlights a case study performed over Libya4 demonstrating that it is possible to achieve a mean accuracy of 3% when simulation are compared with calibrated observations. This activity is part of VITO contribution to CEOS/WGCV/IVOS calibration mission.

***Index Terms*—** Vicarious calibration, desert sites, CEOS/ WGCV/IVOS

1. INTRODUCTION

Accurate calibration of spaceborne imagers is becoming critically important for the derivation of quantitative geophysical information and for the monitoring of key climate variables. In this context, VITO has undertaken the development of an Optical Sensor CAlibration with simulated Radiance (OSCAR) facility dedicated to the routine vicarious calibration of radiometers, and more specifically the future ESA Proba-V mission.

The proposed approach relies on a combination of various vicarious calibration methods based on the exploitation of reflected radiance by clouds, atmospheric molecules or bright desert surfaces. Over bright desert targets, simulated Top-Of-Atmosphere (TOA) Bidirectional Reflectance Factor (BRF) define an absolute reference against which radiometers can be calibrated. These simulations are based on the radiative properties originally proposed by [1]. Several improvements are presented here and concern (*i*) the use of an advanced radiative transfer model that accounts for polarization [2, 3], (*ii*) the improvement of the surface reflectance characterization and (*iii*) the use of a non-spherical aerosol model.

The purpose of this paper is to present these improvements and to evaluate the accuracy with which observations acquired by several polar orbiting imagers, presented in Section (2), can be simulated. These improvements are described in Section (3) and are evaluated in Section (4). This work is performed in the framework of VITO contribution to CEOS/WGCV/IVOS calibration mission using data extracted from ESA Database for Imaging Multi-spectral Instruments and Tools for Radiometric Intercomparison (DIMITRI).

*This work has been funded by BELSPO contract 071220.

Table 1. Number of selected observations N_t in the common spectral bands during the 2006–2009 period over Libya4. Wavelengths are expressed in μm.

BAND	0.44	0.55	0.66	0.84	1.62
VGT	723		700	709	695
AATSR		114	117	119	120
PARASOL	4078	4072	4225	4205	
MODISA	848	864	846	839	822
MERIS	371	378	372	367	

2. SATELLITE DATA

For the evaluation of the simulated TOA reflectance accuracy, a series of observations acquired over Lybia4 [4] by polar orbiting radiometers, *i.e.*, VEGETATION 2, PARASOL, Envisat MERIS and AATSR and finally Aqua/MODIS, during the 2006–2009 period have been processed. These data have been extracted from the ESA DIMITRI data base. The corresponding TOA BRFs $r_o(t,\Omega)$ acquired at time t have been simulated under the same geometry of observation Ω. For each time series of the couple $(r_o(t,\Omega), r_s(t,\Omega))$, where $r_o(t,\Omega)$ and $r_s(t,\Omega)$ stand for the observed and simulated TOA BRF respectively, the following statistics have been derived:

$$\bar{R} = \frac{1}{N_t} \sum_t \frac{r_o(t,\Omega)}{r_s(t,\Omega)} \quad (1)$$

$$\bar{B} = 100\, \frac{1}{N_t} \sum_t \frac{r_o(t,\Omega) - r_s(t,\Omega)}{r_s(t,\Omega)} \quad (2)$$

where N_t is the number of valid observations, *i.e.*, after removal of the outliers at a 2σ confidence interval.

Almost all these radiometers observe in the 0.44, 0.55, 0.66, 0.84 and 1.62μm spectral intervals that are referred to

here as the common spectral bands. For the AATSR observations, only the nadir camera is considered in this study. The number of valid observations used in this study is indicated in Table (1)

3. IMPROVED RADIATIVE TRANSFER MODELLING

3.1. Background

The characterization of the desert site Libya4 [4] surface properties originally relies on the work of [1]. This characterization was based on few months of multi-angular spaceborne observations acquired by ADEOS-1/POLDER in the 0.443, 0.670, 0.765 and 0.865μm spectral bands and ERS2/ATSR2 in the 1.6μm band. The surface BRF model of [5], referred to as RPV, was inverted against these observations corrected from atmospheric scattering and absorption effects. Additionally, the ensemble of bright bare soil spectra of the ASTER spectral library matching these five spectral bands values were used for the interpolation and extrapolation of the surface reflectance in the 0.4–1.8μm spectral interval. Simulation of Top-Of-Atmosphere (TOA) Bidirectional Reflectance Factor (BRF) where performed with the SIXS code[6] using the desert background aerosol model of [7] that assumes spherical particles.

3.2. Radiative transfer model

The improved radiative transfer simulations are now based on the SIXSV code developed by [2]. This code accounts for radiation polarization through the calculation of four components of the Stokes vector, *i.e.*, $\vec{I} = \{I, Q, U, V\}$. The first component, I, describes the intensity of radiation; the other three characterize perpendicular Q, parallel U, and elliptical V polarization. The scattering and absorption properties of aerosols are represented by the single scattering albedo ω_0, and the scattering matrix $P(\Theta)$. This matrix describes the angular polarizing properties of a single-scattering event in the layer [8].

3.3. Surface characterization

The original surface reflectance data set has been derived 10 years ago [1] when only limited space observations were available. An update version of the surface data set has been generated taking advantage of the availability of more than 10 years of surface BRF values derived from MODIS and MISR observations. A new data set has therefore been processed using the approach described in Section (3.1) and is shown in Figure (1), solid line. Both the shape of the BRF and the magnitude of the surface albedo are slightly different in this new data set. In the current configuration, the surface is assumed depolarized though typical polarization over land surfaces such as sand is in the range of 0%-15% [9].

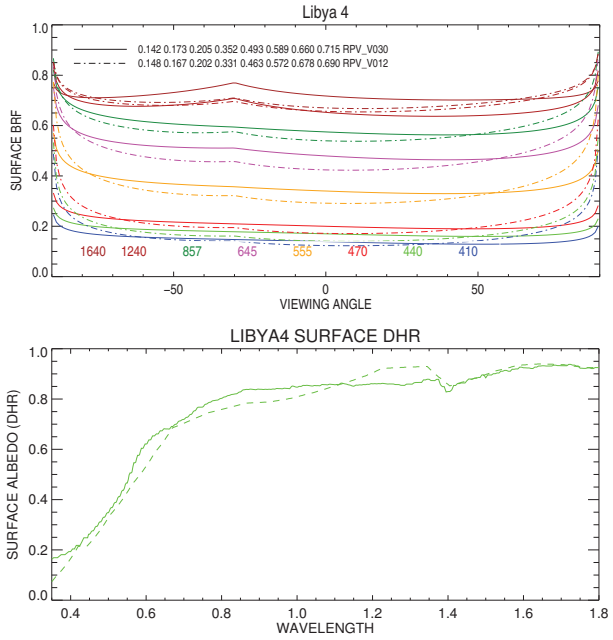

Fig. 1. Top: Surface BRF in the principal plane over Libya4 in the following wavelengths: 410, 440, 470, 555, 645, 857, 1240 and 1640 nm. The original values are shown with dash-dotted lines. The proposed improvements are shown with solid lines. Bot: Surface albedo (DHR) over Lybia4. The original values are shown with dashed lines and the proposed improvements are shown with solid lines.

3.4. Aerosol model

An original method has been developed for the systematic analyse of AERONET data [10] for the derivation of an aerosol model specifically dedicated to the Sahara region. Each valid AERONET observation, which has been defined according to the same criteria as in [11] and [12] could be represented by a spectral path or trajectory in a two dimensional space defined by the asymmetry parameter g and the single scattering albedo ω_0. This trajectory writes $(g(\lambda), \omega_0(\lambda))$ considering four wavelengths: 0.44, 0.67, 0.87 and 1.02μm. The mean spectral trajectory has been estimated considering all AERONET stations available in the Sahara region. The corresponding mean aerosol model is shown on Figure (2). This model is composed of spheroid particles whose single scattering properties are derived with the method of [8].

4. EVALUATION

The overall results of the mean relative difference $\bar{B}$ between satellite TOA BRFs and SIXSV simulations over Libya4 are shown on Table (2), together with the mean and range of $\bar{B}$ values in each spectral band. As can be seen, simulations performed in the 0.44μm and 0.55μm bands systematically

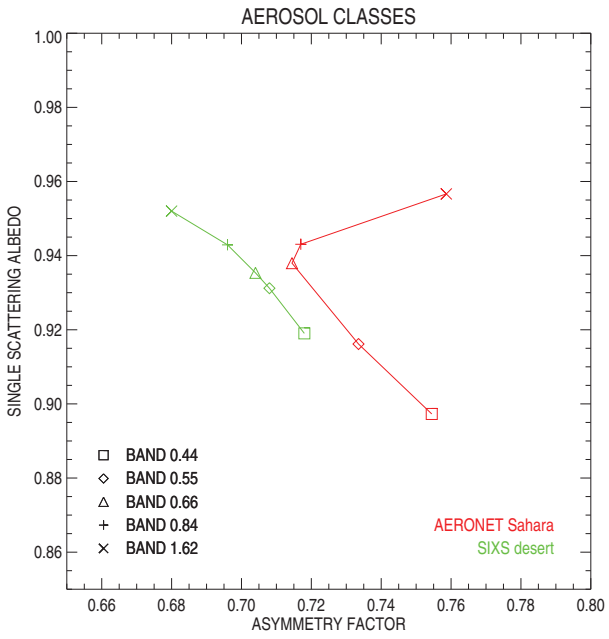

Fig. 2. Representation of the new aerosol model (red) with the Shettle model in the single scattering albedo - asymmetry parameter space in the common spectral intervals. See text for details.

overestimate observations. Such a clear behaviour does not occur in the other spectral intervals. However, in all common spectral bands, there is a very good consistency between AQUA-MODIS, MERIS and PARASOL radiometers, where the difference in the range of $\bar{B}$ values for each common spectral band does not exceed 1.5%, which indicates that these radiometers are consistently calibrated. VEGETATION 2 observations underestimate TOA BRF simulations to the exception of the blue band. AATSR TOA BRFs restricted to nadir camera observations are systematically lower than simulated ones. The mean $\bar{B}$ values derived considering all radiometers show that it is possible to simulate TOA BRF within 3% accuracy when enough observations are taken into account. The range of $\bar{B}$ values shows that there is still room to improve the calibration consistency among these radiometers.

Table 2. Mean relative difference in percent $\bar{B}$ between satellite TOA BRFs and SIXSV simulations over Libya4 during the 2006–2009 period. Wavelengths are expressed in μm.

BAND	0.44	0.55	0.66	0.84	1.62
VGT	+0.79		-3.14	-2.46	-1.13
AATSR		+3.89	+2.81	+4.21	+3.82
PARASOL	+3.08	+0.71	-0.23	-0.00	
MODISA	+3.36	+2.95	+0.58	+1.55	+2.05
MERIS	+2.60	+2.80	+1.41	+1.50	
Mean	2.46	2.59	0.29	0.96	1.58
Range	2.57	3.18	5.95	6.50	4.95

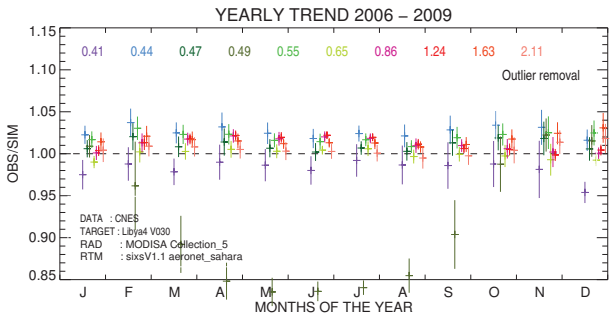

Fig. 3. Monthly ratio $\bar{R}_M$ (horizontal bars) between observations and simulations for the AQUA-MODIS instrument over the Libya4 site. The vertical bars show the standard deviation of $\bar{R}_M$ for each month.

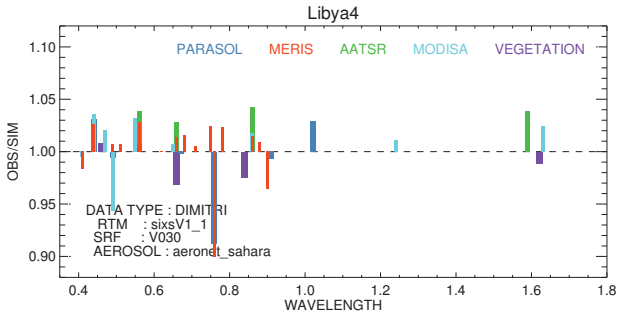

Fig. 4. Overall results of the ratio $\bar{R}$ for the processed satellite data over the Libya4 site.

We next examine the seasonal variations of the ratio $r_o(t)/r_s(t)$. For that purpose, the monthly mean value of that ratio $\bar{R}_M$ has been computed during the period of acquisition. Results are shown on Figure (3) for the AQUA-MODIS instrument. The 0.41μm band show a small seasonal cycle as oppose to all other bands that do no exhibit any seasonal trends.

Finally, the ratio $\bar{R}$ overall results are presented on Figure (4), considering now all spectral bands of each radiometer. These results confirm the good consistency between AQUA-MODIS, MERIS and PARASOL radiometers. There are still rooms for the improvement of these results in particular (*i*) in in the 0.41–0.47μm spectral region where simulations in both the 0.41 and 0.47μm spectral bands underestimate observations which are overestimates in the 0.44μm spectral band and (*ii*) the observations in the 0.55μm spectral band tends to be underestimated by simulations. The proposed method does not provide satisfactory results for the calibration of spectral band located in the oxygen-a and -b spectral regions.

5. CONCLUSIONS

We present here an improvement of bright desert radiative data set[1] which is used for the generation of an absolute calibration reference. This improvement is illustrated on a case study performed over Libya4. This work has been performed in the context of an evaluation of the ESA DIMITRI initiative under the umbrella of CEOS/WGCV/IVOS calibration activities. These improvements include atmospheric polarization processes, the consideration of spheroidal aerosol particles and finally the surface BRF. These improved simulated TOA BRFs represent the reference against which radiometers can be calibrated or their calibration compared.

It has been shown that, on the average, it is possible to simulate observations acquired by polar orbiting radiometers over Libya4 with an accuracy of 3%, the largest error being observed in the blue spectral region. The reason of this discrepancy is still an open issue that requires further work.

This work also reveals differences between the calibration of these radiometers, in particular for the VEGETATION 2 and Envisat/AATSR instruments.

Finally, it might be worthwhile to expand this work to all desert targets identified by [4] in order to further increase the simulation accuracy, reducing the impact of uncorrelated errors.

6. REFERENCES

[1] Y. M. Govaerts and M. Clerici, "Evaluation of radiative transfer simulations over bright desert calibration sites," *IEEE Transactions on Geoscience and Remote Sensing*, vol. 42, no. 1, pp. 176–187, 2004, IEEE Trans. Geosci. Remote Sens.

[2] S. Y. Kotchenova, E. F. Vermote, R. Matarrese, and Jr. Klemm, F. J., "Validation of a vector version of the 6s radiative transfer code for atmospheric correction of satellite data. part i: Path radiance," *Applied Optics*, vol. 45, pp. 6762–6774, 2006, DOI: 10.1364/AO.45.006762.

[3] S. Y. Kotchenova and E. F. Vermote, "Validation of a vector version of the 6s radiative transfer code for atmospheric correction of satellite data. part ii. homogeneous lambertian and anisotropic surfaces," *Applied Optics*, vol. 46, pp. 4455–4464, 2007, DOI: 10.1364/AO.46.004455.

[4] H. Cosnefroy, Briottet, X., M. Leroy, P. Lecomte, and R. Santer, "A field experiment in saharan algeria for the calibration of optical satellite sensors," *Int. J. Remote Sensing*, vol. 18, no. 16, pp. 3337–3359, 1997, International Journal of Remote Sensing.

[5] H. Rahman, B. Pinty, and M. M. Verstraete, "Coupled surface-atmosphere reflectance (CSAR) model. 2. Semiempirical surface model usable with NOAA Advanced Very High Resolution Radiometer data," *Journal of Geophysical Research*, vol. 98, no. D11, pp. 20,791–20,801, 1993, J. Geophys. Res.

[6] E. Vermote, D. Tanr, J. L. Deuze, M. Herman, and J. J. Morcrette, "Second simulation of the satellite signal in the solar spectrum (6S): User's guide, version 1," Tech. Rep., Dept. of Geography, Univ. of Maryland, and NASA-Goddard Space Flight Center - Code 923, Greenbelt, MD 20771, USA, April 18, 1994 1995, e.

[7] E. P. Shettle and R. W. Fenn, "Models for the aerosols of the lower atmosphere and the effects of humidity variations on their optical properties," Tech. Rep. AFGL-TR-79-0214, U.S. Air Force Geophysics Laboratory, U.S. Air Force Geophysics Laboratory, 1979 1979.

[8] O. Dubovik, "Optimization of numerical inversion in photopolarimetric remote sensing," in *Photopolarimetry in Remote Sensing*, G. Videen, Y. Yatskiv, and M. Mishchenko, Eds., vol. 161, pp. 65–106. Springer Netherlands, 2006.

[9] K. N. Liou, *An introduction to Atmospheric Radiation*, Academic Press, London, second edition, 2002.

[10] B. N. Holben, T. F. Eck, I. Slutsker, D. Tanre, J. P. Buis, A. Setzer, E. Vermote, J. A. Reagan, Y. J. Kaufman, T. Nakajima, F. Lavenu, I. Jankowiak, and A. Smirnov, "AERONET-a federated instrument network and data archive for aerosol characterization," *Remote Sensing of Environment*, vol. 66, pp. 1–16, 1998, Remote Sensing of Environment.

[11] O. Dubovik, B. Holben, T. F. Eck, A. Smirnov, Y. J. Kaufman, M. D. King, D. Tanre, and I. Slutsker, "Variability of absorption and optical properties of key aerosol types observed in worldwide locations," *Journal of the Atmospheric Sciences*, vol. 59, no. 3, pp. 590–608, 2002.

[12] R. Levy, L. Remer, and O. Dubovik, "Global aerosol optical properties and application to moderate resolution imaging spectroradiometer aerosol retrieval over land," *Journal of Geophysical Research*, vol. 112, no. D13210, pp. doi:10.1029/2006JD007815, 2007, JGR.